Global and Planetary Change 203 (2021) 103539

Contents lists available at ScienceDirect

Global and Planetary Change

journal homepage: www.elsevier.com/locate/gloplacha

Fate of terrigenous organic carbon in muddy clinothems on continental shelves revealed by stratal geometries: Insight from the Adriatic sedimentary archive

Claudio Pellegrini [a,*], Tommaso Tesi [b], Juergen Schieber [c], Kevin M. Bohacs [d], Marzia Rovere [a], Alessandra Asioli [a], Alessio Nogarotto [e], Fabio Trincardi [a]

[a] Istituto di Scienze Marine (ISMAR-CNR), Via Gobetti 101, 40129 Bologna, Italy
[b] Istituto di Scienze Polari (ISP-CNR), Via Gobetti 101, 40129 Bologna, Italy
[c] Department of Geological Sciences, Indiana University, 1001 East 10th Street, Bloomington, Indiana, USA
[d] KMBohacs GEOconsulting, Houston, TX, USA
[e] Dipartimento di Scienze Ambientali, Informatica e Statistica, Università Ca' Foscari di Venezia, Via Torino 155, 30172 Venezia, Italy

ARTICLE INFO

Editor: Matenco Liviu

Keywords:
Continental shelf
Organic carbon
Depositional processes
Delta-clinoform
Little Ice Age

ABSTRACT

Continental shelves host 90% of modern Organic Carbon (OC) burial and play a key role in the sequestration of terrigenous OC over geological timescales. The efficiency of OC burial in these systems, however, varies greatly depending on the duration of exposure to oxic-suboxic conditions during sediment transport. In this study, we use observations across a wide range of stratigraphic and sedimentological scales coupled with geochemistry data from muddy shelf deposits along the western Adriatic to investigate the relation between sediment transport and burial of terrigenous (land-derived) fraction of OC (OC_{Terr}). Our analysis focused on the Little Ice Age (LIA, 1500–1850 CE) interval, which was characterized by wet, cold, and stormy weather conditions, before the time of widespread regulation and damming of rivers. On the Adriatic shelf, LIA deposits are organized as clinothem: strata that dip gently seawards. The LIA clinothem becomes progressively steeper and deeper from north to south. Basin-scale seismic-stratigraphic analysis and biogeochemical data show evidence of elongated stratal units associated with low OC_{Terr} content in the northern sector of the LIA clinothem, whereas farther south, where clinoforms are steeper, the LIA clinothem exhibits wavy stratal units with limited cross-shelf continuity and high OC_{Terr} concentrations. Based on these data we infer two contrasting scenarios for OC_{Terr} deposition during the LIA: 1) protracted sediment redistribution under the influence of coastal currents with efficient OC_{Terr} degradation prior to final burial in the northern sector; and (2) rapid deposition of OC_{Terr}-rich event beds as a result of flood-driven hyperpycnal flows with limited dispersion across the shelf in the southern sector. The latter scenario of deposition resulted in scattered hot spots of OC_{Terr} burial along the apparently homogeneous western Adriatic shelf deposit. Our work documents significant lateral variability of a fine-grained system in which hot spots of OC_{Terr} can be preserved in scattered prodelta bedsets (<1 km in across-shelf lateral continuity) over a 600 km long shelf. Shelfal clinothems worldwide should not be considered as homogeneous pools of OC_{Terr} because of the influence of river, storm, and oceanic currents.

1. Introduction

The sequestration of organic carbon (OC) on continental shelves – ~90% of the global OC burial in the ocean – contributes to the regulation of atmospheric CO_2 concentrations over geological time scales (Berner, 1982; Hedges et al., 1997; Aller and Blair, 2006; Blair and Aller, 2012; Bauer et al., 2013; Bianchi et al., 2016, 2018). Yet, although there is general agreement that continental shelves are the largest sink of both terrigenous and marine OC in the global ocean (Hedges, 1992; Hedges and Keil, 1995; Luisetti et al., 2020), many studies of early diagenesis in modern sediments found that only a minor fraction of the OC escapes degradation on continental shelves at present (Blair and Aller, 2012). Even Terrigenous OC (OC_{Terr}), generally considered refractory to oxidation, exhibits surprisingly little evidence of persistence in present-

* Corresponding author.
E-mail address: claudio.pellegrini@bo.ismar.cnr.it (C. Pellegrini).

https://doi.org/10.1016/j.gloplacha.2021.103539
Received 7 November 2020; Received in revised form 4 June 2021; Accepted 4 June 2021
Available online 9 June 2021

day marine sediments (Hedges et al., 1997; Cai, 2011). This limits our ability to predict the OC_{Terr} flux responses to changes in climate and land use, even in river delta clinothems (sensu Pellegrini et al., 2020).

Among the different factors that control OC_{Terr} burial (e.g. intrinsic reactivity, matrix protection, and priming effects), the time spent under oxic-suboxic conditions before burial in sediments exerts a first-order control on the fate of OC (Keil et al., 2004; Zonneveld et al., 2010; Smith et al., 2015; Cui et al., 2016; Bao et al., 2016, 2018; Bianchi et al., 2018; Bröder et al., 2018). In this study, we focus on the 600-km-long Adriatic shelf deposit to understand how the protracted transport of OC_{Terr} over the Adriatic margin can affect its ultimate preservation. The Adriatic shelf is shaped by storm waves and southward marine currents that laterally redistribute sediments supplied by the Po River and an array of Apennine steep rivers (Fig. 1). The Adriatic shelf deposit is constituted by coalescing delta-scale clinothems that appear skewed (sensu Korus and Fielding, 2015) relative to the main river entry points (Cattaneo et al., 2003; Pellegrini et al., 2015), and shows a progradational nature common to several other muddy systems affected by currents (Amazon River, Nittrouer et al., 1996; Ganges–Brahmaputra River, Michels et al., 1998; Eel River, Bentley and Nittrouer, 2003; Fly River, Walsh et al., 2004, Goñi et al., 2008; Yellow River, Liu et al., 2004; Mekong River, Xue et al., 2010; Mississippi-Atchafalaya rivers, Bianchi et al., 2011, Denommee et al., 2016).

Dams built along the Italian rivers since the late 1940s have profoundly changed the natural sediment flux by reducing sediment load of up to 20% (Syvitski et al., 2005; Syvitsky and Kattner, 2011). In order to characterize the fundamental mechanisms that drive sediment and OC_{Terr} accumulation on the Adriatic shelf, we circumvented the effect of human-induced modern reduction of riverine sediment flux by analyzing strata deposited during the Little Ice Age (LIA, 1500–1850 CE; Fig. 1). The LIA is considered as a crucial interval of global change that affected the climate system with fluctuations that include glacier extent, precipitation, and thermohaline and atmospheric circulation (e.g. Fagan, 2019; Broecker, 2000). At the Mediterranean scale, the LIA was characterized by cold, wet, and stormy conditions that significantly increased the land-to-ocean exchange of sediment (Camuffo et al., 2000; Grove, 2001; Dezileau et al., 2011; Comiti, 2012; Anthony et al., 2014) and affected deltaic architecture (e.g. Cattaneo et al., 2003; Fanget et al., 2014). In addition, changes in the vegetation, soil stability, and human-influenced deforestation within watersheds in response to the cold period enhanced sediment yields (Giosan et al., 2012; Maselli and Trincardi, 2013; Renaud et al., 2013; Kulkarni et al., 2018; Mariani et al., 2019). Overall, the relatively high sediment input makes the LIA clinothem an ideal laboratory for investigating the fate of OC_{Terr} along the land-ocean continuum.

Our overarching goals were to (1) decipher the link between subtle

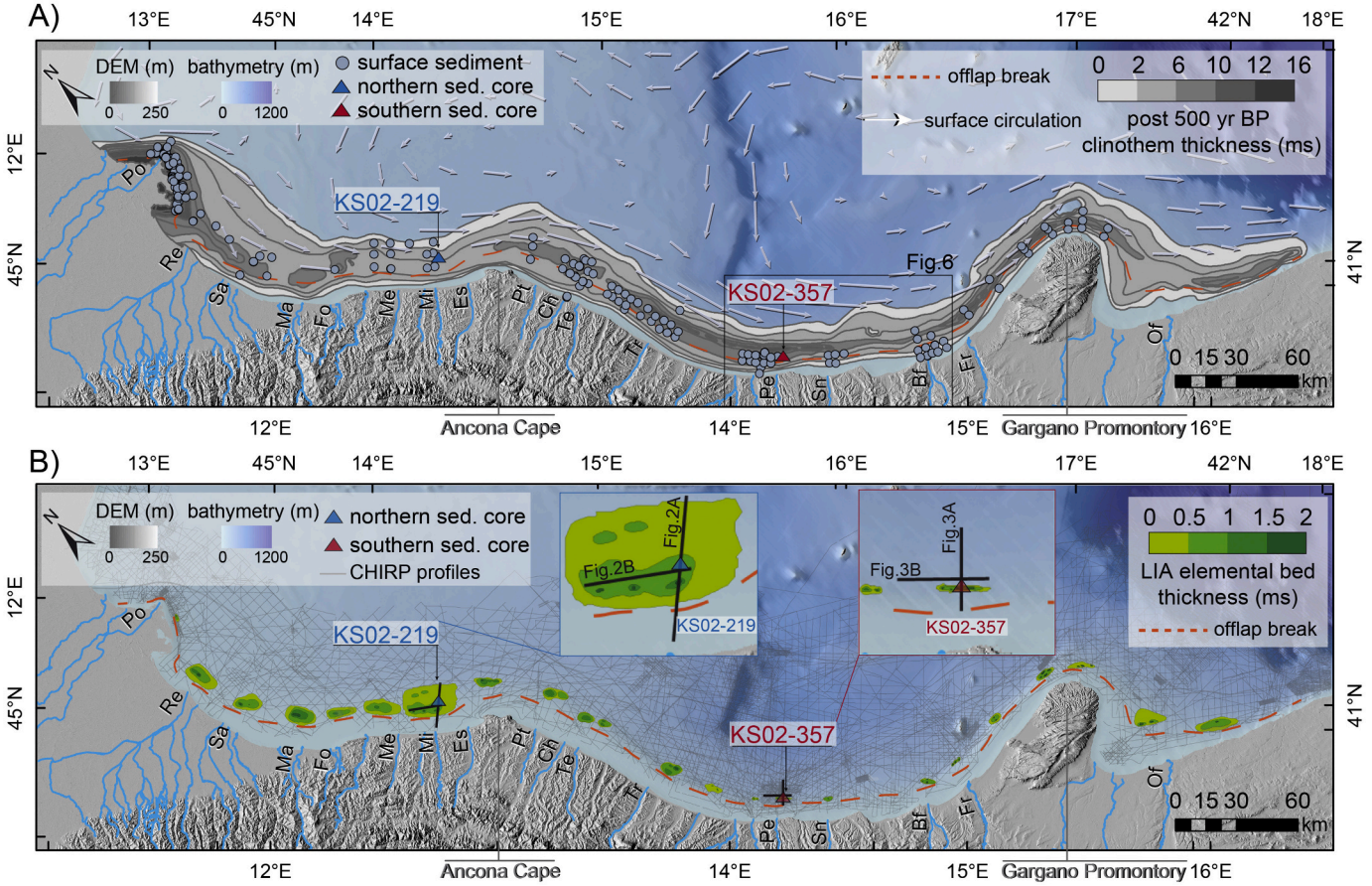

Fig. 1. Digital elevation model for the Adriatic Sea and Italian catchments. Main Italian rivers are represented with these abbreviations: Po River (Po), Reno River (RE), Savio River (Sa), Marecchia River (Ma), Foglia River (Fo), Metauro River (Me), Misa River (Mi), Esino River (Es), Potenza River (Pt), Chienti River (Ch), Tronto River (Tr), Pescara River (Pe), Sangro River (Sn), Biferno River (Bf), Fortore River, (Fr), and Ofanto River (Of). A) Thickness distribution of the shelf clinothem deposited in the last 500 yr and spanning the Little Ice Age (LIA). Orange dashed line represents the position of clinothem offlap break. Arrows represent surface circulation (averaged measurements of drifter velocities; Poulain, 2001). Circles and triangles represent the location of surface sediments and sediment cores, respectively, acquired along the western Adriatic shelf. The northern sector extends between Po River and Ancona Cape, and the southern sector from Ancona Cape down to Gargano Promontory. B) Green polygons denote thickness and continuity of LIA elemental beds (greatest in the northern sector). Inset: the smallest lateral extent of elemental bed is recorded offshore the Pescara River (Pe). (For interpretation of the references to colour in this figure legend, the reader is referred to the web version of this article.)

stratal architecture and OC composition in skewed muddy clinothem deposits and (2) explore whether stratal architecture can be used as a diagnostic tool to infer the fate of OC_{Terr}. We used an integrated approach, which combines geochemical data (bulk carbon isotopes and terrigenous biomarkers) with observations across a wide range of sedimentological scales (from μm to m). In addition, seismic-stratigraphic analysis at high resolution (dm to m) provided key information on basin-scale stratal geometries and sediment-transport modes along the LIA clinothem. Finally, we applied the concept of hot spots and hot moments (sensu McClain et al., 2003 and Bianchi et al., 2018) for burial of OC_{Terr} at the Adriatic land-ocean interface. We refer to hot spots as elemental beds that show high OC_{Terr} concentration relative to the surrounding sediments, and hot moments as short periods of time within the LIA related to river floods.

2. Background

2.1. Sediment provenance, flux, and transport along the northern and southern sectors

The late Holocene deposit on the Adriatic shelf comprises a variety of sedimentary systems that include rivers that drain the Alps and Apennine mountains and supplied coalescing deltas. The Po River acts as a major sediment conveyor from the Alps and northern Apennines, while Apennine rivers have, individually, substantially smaller drainage areas but, as a whole, account for twice as much the sediment yield from the Po, because of the poorly consolidated and erodible lithology in their steep catchments (Cattaneo et al., 2003; Amorosi et al., 2016). Thus, at basin scale, the Po and the Apennine rivers act as a series of adjacent point sources of sediment input nourishing the Adriatic basin (Fig. 1).

The Adriatic basin water mass is characterized by energetic geostrophic circulation currents of thermohaline origin (Artegiani et al., 1997), intense Ekman transport and internal waves (Puig et al., 2007), and a storm wave base ~35 m deep (Chiggiato, personal comm.). Sediment dispersion is driven mainly by a cyclonic surface-water gyre, enhanced by energetic subdecadal events of dense-water formation and southward flow along bathymetric contours (Benetazzo et al., 2014; Chiggiato et al., 2016). As a result of these current forcings, sediment accumulated in a laterally continuous (600-km-long) muddy clinothem along the Italian coast characterized by depocenters parallel to the coastline and confined on the mid-shelf (Fig. 1).

Based on the fate of the sediment on the shelf, the Adriatic has been subdivided into two main depositional settings (Palinkas and Nittrouer, 2006): (i) the northern sector, between Po River and Ancona Cape, where reworking exceeds sediment supply by local rivers resulting in sediment bypassing this sector (input 16.9 Tg y^{-1} vs sediment accumulation 7.5 Tg y^{-1}), compared to the (ii) southern sector, between Ancona Cape and the Gargano Promontory, where net sediment accumulation is greater than the input from local rivers (input 7.8 Tg y^{-1} vs 13.9 Tg y^{-1} sediment accumulation; Frignani et al., 2005). The two depositional settings show different stratal geometry as well. In the northern sector, late-Holocene stratal configuration shows prograding clinoforms with few internal convergences (Cattaneo et al., 2003). In this shallow (< 100 m) sector, winds generate energetic waves that exert large bed shear stresses capable of re-suspending fine-grained material (Traykovski et al., 2007; Harris et al., 2008). In the southern sector, undulating strata have been observed in the late-Holocene clinothem (including the LIA interval; Cattaneo et al., 2004) offshore of steep and mud-rich Apennine rivers, whose intense seasonal runoffs may produce high-density fluvial flows (Syvitski and Kettner, 2007), and where bottom-current activity affects the foreset (Puig et al., 2007). Undulating strata have been documented in other prodeltaic deposits worldwide (e.g. Bornhold and Prior, 1990; Urgeles et al., 2007) but their origins remain a matter of debate (deformational features generated by creeping (Correggiari et al., 2001; Lee and Chough, 2001) or depositional features generated by high-density sediment flows flowing on the shelf (Trincardi and Normark, 1988; Lee et al., 2002; Puig et al., 2007; Slootman and Cartigny, 2020)).

2.2. The late-Holocene Adriatic clinothems

The late-Holocene Adriatic deposit shows delta-scale clinoforms (sensu Patruno and Helland-Hansen, 2018; Pellegrini et al., 2020), like those recognized seaward of major rivers worldwide (Korus and Fielding, 2015 for a review). Clinoforms and clinoform-bounded sedimentary units, clinothems, are characterized by three geometric elements: the topset represents the most low-angle and proximal sector; the foreset is the intermediate sector and is characterized by the steepest morphological gradient; the bottomset comprises the near-horizontal basinward sector. The morphological break in slope at the topset–foreset transition is called offlap-break (or rollover point) and coincides with the point of maximum curvature (Pirmez et al., 1998; Patruno et al., 2015; Pellegrini et al., 2020).

The late-Holocene Adriatic clinothem comprises strata that extend from subaerial deltas (Trincardi et al., 2020) to their coeval fine-grained subaqueous deposits (i.e. compound clinothems, Cattaneo et al., 2007; Pellegrini et al., 2015). The Adriatic subaqueous clinothems have a subaqueous topset, a rollover point in water depths of less than 10 m in the north and up to 30 m in the south, and a foreset which progressively increases in steepness and relief in the down current direction (i.e. from the Po River to the Gargano Promontory; Cattaneo et al., 2003, 2007). It is important to highlight that, in the case of the late Holocene Adriatic clinothem (ca. 6000 y), one third of its volume (60 km^3) accumulated during just the ~350 years of the LIA (1500–1850 CE, supp. material), as the result of a greater sediment supply to the basin compared to underlying clinothems (Cattaneo et al., 2003; Piva et al., 2008). The base and top of the LIA clinothem can be traced and mapped over >600 km along shelf (Figs. 1 and DR1).

3. Methods and datasets

3.1. Seismic-stratigraphic analysis

Seismic-stratigraphic analysis allows basin-scale correlations and quasi-three-dimensional rendering of stratal components based on 30,000 km of CHIRP-sonar profiles (2–7 kHz outgoing signal) with a typical line spacing of 3 km and a vertical resolution of 20–30 cm (Figs. 2 and 3). Age constraints on the late-Holocene Adriatic clinothem came from calibrated ^{14}C dates, short-lived radionuclides analyses (^{210}Pb), tephra identification, and dated key bio-events from continuous recovery boreholes and sediment cores located along the depocenter of the late-Holocene Adriatic clinothem (Fig. DR1 and Tabs. DR1, DR2). The regional stratigraphic correlation is further corroborated from CHIRP-sonar profiles, whole-core magnetic susceptibility, and Saturation Isothermal Remnant Magnetization (SIRM; Oldfield et al., 2003; Vigliotti et al., 2008).

At seismic-profile scale, the smallest-scale stratal components (which we call "elemental beds") were identified with a vertical resolution of ~20 cm (i.e. each seismic reflection was considered to be an elemental bed). The elemental beds are stacked to form bedsets, and are bounded by chronostratigraphically significant marine-flooding surfaces (top and base of the LIA clinothem) according to original definitions of the hierarchy of stratal units (Campbell, 1967; Van Wagoner et al., 1990). Thus, elemental beds are the building blocks of the LIA clinothem (Figs. 2 and 3). Geosuite AllWorks 2019R2 and ESRI ArcGIS 10.5 software were used to identify reflection terminations and map thickness between two stacked and subsequent elemental beds deposited during the LIA (green polygons in Fig. 1B). Since not all of the elemental beds can be represented readily in plan view, we provide a tabular compilation and statistical characterization of the distribution of their dimensions along the LIA clinothem (Fig. 4).

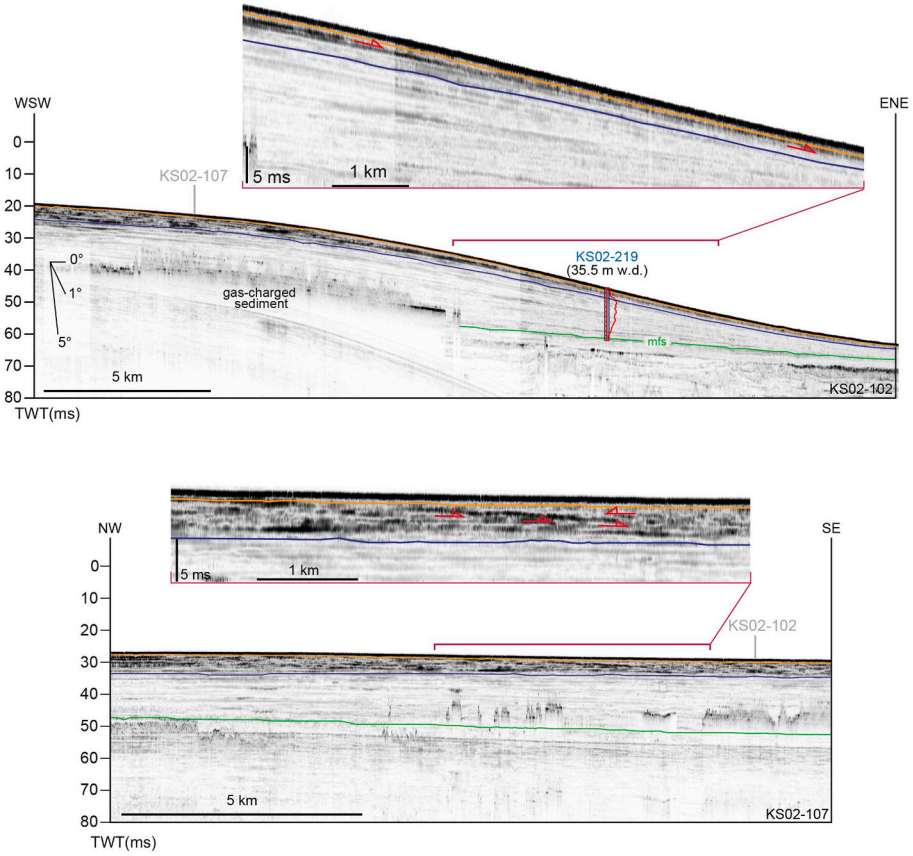

Fig. 2. Seismic-reflection profiles (CHIRP, vertical resolution of ca. 0.2 m) from the northern sector of the Adriatic shelf (see Fig. 1B for profile location). Top: across-shelf profile (KS-102) shows distinct sigmoidal clinoform geometries and the position of sediment core KS02–219 in the foreset. Bottom: along-shelf profile (KS-107) shows subparallel elongated reflections (each seismic reflection represents an 'elemental bed'). Successive elongated reflections show a shingled progradational configuration. Green horizon marks the maximum flooding surfaces (mfs) at the base of the late-Holocene clinothem. Blue and orange horizons mark the base and top of the LIA clinothem, respectively. Insets: red arrows show reflection terminations of the elemental bedsets. (For interpretation of the references to colour in this figure legend, the reader is referred to the web version of this article.)

3.2. Down-core geochemistry and sedimentary structure analyses

Sedimentological analyses on selected piston sediment cores (recovery >90%) were conducted at different resolutions from m to μm-nm scale. The KS02–219 and KS02–357 sediment cores were collected in prodeltaic strata at 35.5 m and 50 m water depth in the northern and southern Adriatic. Of the 35 cores available from the study area (Fig. DR1), these two cores were chosen as most representative in terms of sedimentary structures and seismic facies of the LIA clinothem and optimally located in the northern and southern sectors to test our interpretations. Sediment-core description, coupled with high-resolution digital X-ray images, was used to characterize subtle sedimentary structures in fine-grained sediments. A subset of samples, characterized by evident changes in the texture, was selected for Scanning Electron Microscope (SEM) analyses to detect diagnostic sedimentary structures and reconstruct the main sedimentary processes. SEM samples were stabilized with Spurr resin after removal of pore water with acetone (Schimmelmann et al., 2015), and ion-milled (Schieber, 2013).

Sedimentary organic carbon in KS02–219 and KS02–357 cores was characterized at bulk and molecular levels. Stable carbon isotopes ($\delta^{13}C$) were measured via EA-IRMS (Elemental Analyzer-Isotope Ratio Mass Spectrometry) following the method documented by Tesi et al. (2006). Briefly, freeze-dried grounded samples were transferred in silver caps and acidified (1.5 M HCl) to remove the inorganic fraction. Analyses were carried out using a Finnigan Delta Plus XP mass spectrometer directly coupled to a Thermo Fisher Scientific FLASH 2000 IRMS element analyzer via a ConFlo III interface for continuous flow measurements. Standard deviation based on replicates of reference standard (IAEA-CH7) is $< \pm 0.2$‰.

Lignin phenols (terrestrial biomarkers, Gordon and Goñi, 2003) were quantified according to the method presented in Tesi et al. (2006) using microwave-assisted alkaline CuO oxidation. Briefly, homogenized subsamples of around 300 mg were oxidized, an internal standard added, acidified to pH 1, and extracted. Extracts were derivatized with bis(trimethylsilyl) trifluoroacetamide and 1% trimethylchlorosilane to silylate exchangeable hydrogens and analyzed with a gas chromatograph mass spectrometer (Agilent 7820A) using a programmed temperature increase from 60 to 300 °C. Quantification of the samples was based on the comparison of key ions to commercially available standards. Concentrations of CuO oxidation products were normalized to the organic carbon content of the sample and are reported as mg/g OC.

3.3. Terrigenous and marine organic carbon end-members

We compiled stable carbon isotopes ($\delta^{13}C$) data from published studies on the modern (<20 yr) supply and deposition of OC_{Terr} (Fig. 5) along the Adriatic clinothem to define the terrigenous end-member and contextualize OC_{Terr} burial within the LIA clinothem building on the well-known modern sediment dynamics (Frignani et al., 2005; Palinkas and Nittrouer, 2006). We used an integrated approach compiling together Po River suspended sediments collected during the 2011 flood event (Tesi et al., 2013a; $n = 42$ samples), river-bed sediments from the Apennine rivers collected in 2005 (Tesi et al., 2006; $n = 10$ samples), Po River flood deposits sampled in 2000 and 2009 (Tesi et al., 2011, 2012; $n = 44$ samples; Fig. 5). Regardless of their different origins and nature, all terrigenous samples show the depleted $\delta^{13}C$ signature typical of land-derived material. All values were then averaged (-26.46 ± 0.44‰) to define the $\delta^{13}C$ terrigenous end-member. Lastly, we used the marine $\delta^{13}C$ end-member (-20.4‰) suggested by Tesi et al. (2006) to run the source-apportionment model.

First we defined the terrigenous (i.e. from the continent) and marine signatures (i.e. in-situ production), then we assessed the relative OC_{Terr} content in the LIA clinothem using the following two end-member mixing model:

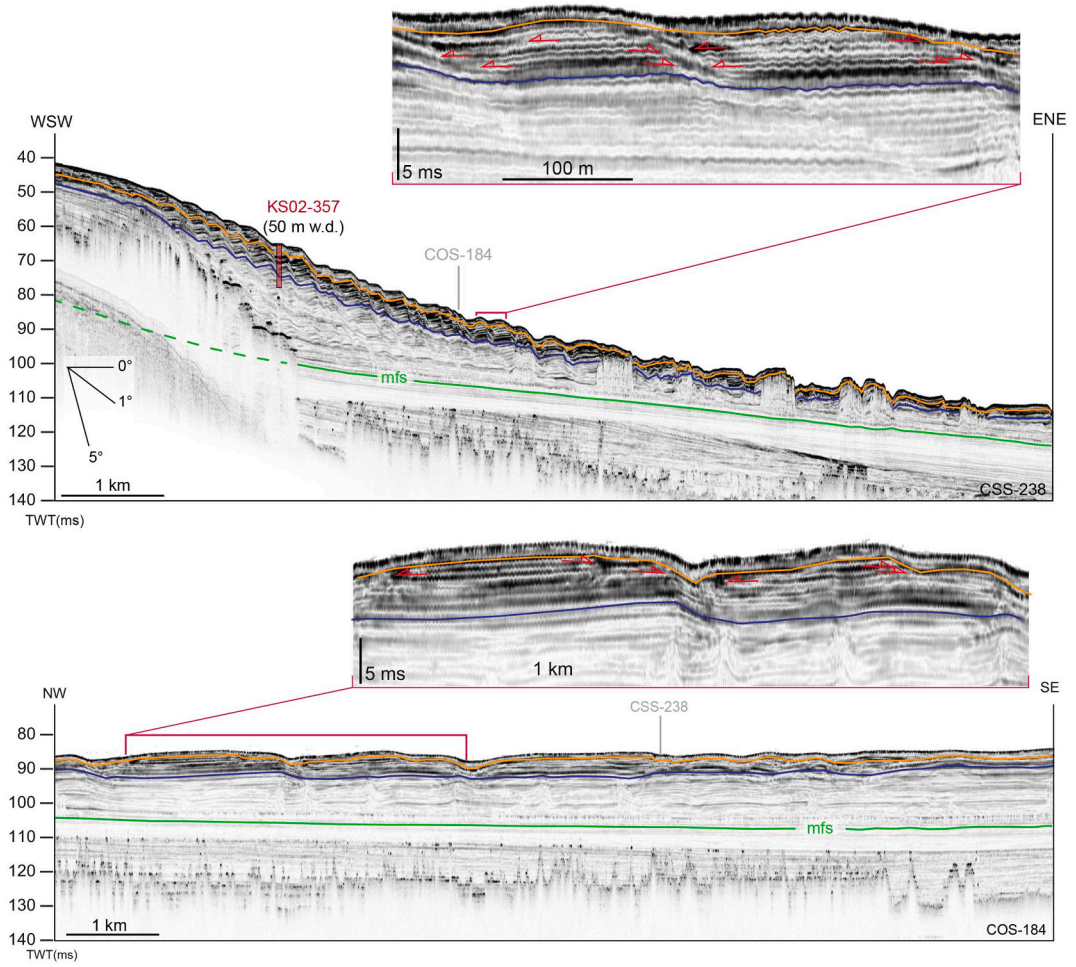

Fig. 3. Seismic-reflection profiles (CHIRP, vertical resolution of ca. 0.2 m) from the southern sector of the Adriatic shelf (see Fig. 1B for profile location). Top: across-shelf profile (CSS-238) shows sigmoidal clinoform characterized by undulations and the position of sediment core KS02–357 in the foreset. Bottom: along-shelf profile (COS-184) shows wavy subparallel reflections (each seismic reflection represents a bed). Green horizon marks the maximum flooding surface (mfs) at the base of the late-Holocene clinothem. Blue and orange horizons mark the base and top of the LIA clinothem, respectively. Insets: red arrows show reflection terminations of the elemental beds, which constitute the Little Ice Age (LIA) deposit. Note the overall small lateral continuity of the reflections. (For interpretation of the references to colour in this figure legend, the reader is referred to the web version of this article.)

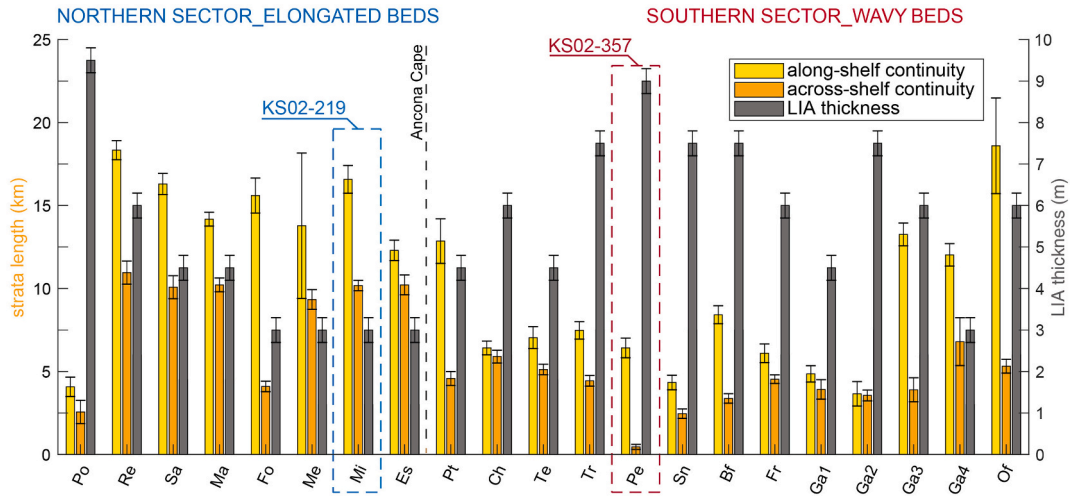

Fig. 4. Bar graph of elemental-bed continuity (length along-shelf and across-shelf) encountered at foreset of the LIA clinothem and thickness of the LIA clinothem along the western Adriatic shelf offshore the main river entry points (see Fig. DR1). Despite the contrasting LIA thicknesses between northern and southern sectors (grey bar), wavy beds (southern sector) show smaller lateral continuity than elongated beds (northern sector). Sediment core KS02–357 was retrieved offshore Pescara River (Pe) where across-shelf bed continuities shrink to <400 m.

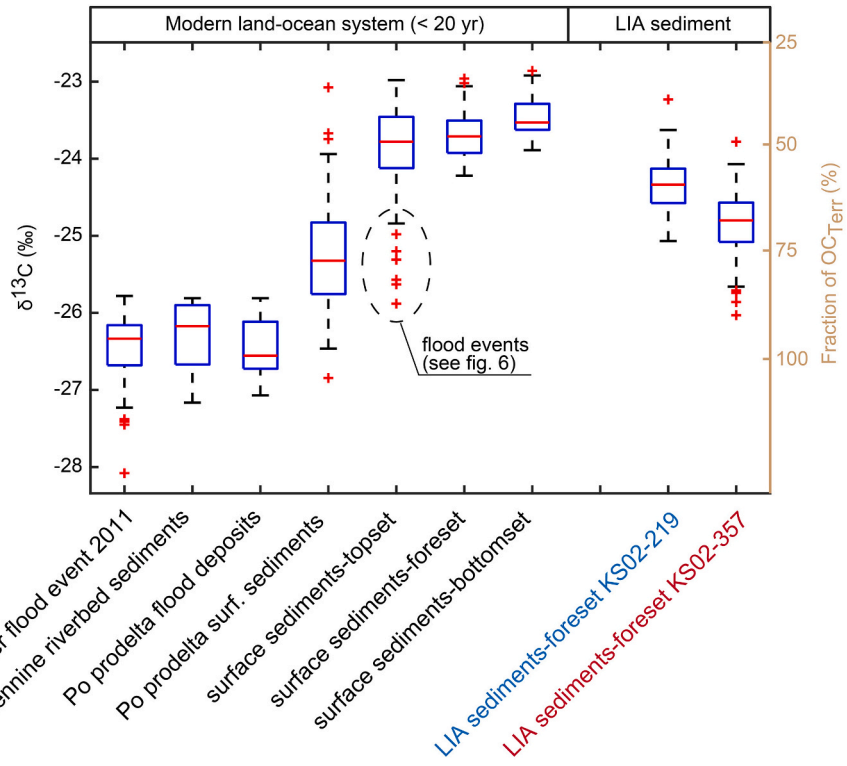

Fig. 5. Collection of $\delta^{13}C$ data from surface sediments along the source-to-sink Adriatic system. Data were grouped as follows: Po River suspended sediment samples (Tesi et al., 2013a), Apennine riverbed sediments (Tesi et al., 2006), Po prodelta flood deposits (Tesi et al., 2011), Po prodelta surface sediments (Tesi et al., 2013b), surface sediments from the Adriatic clinothem topset, foreset, and bottomset (Tesi et al., 2013b), and LIA clinothem (sediment cores KS02–357 and KS02–219). The central red line shows the median. Bottom and top edges of the box indicate the 25th and 75th percentiles, respectively. The whiskers (black line) extend to the most extreme data points not considered outliers, and the outliers are plotted individually as red crosses. (For interpretation of the references to colour in this figure legend, the reader is referred to the web version of this article.)

$$\delta^{13}C_{sample} = F_{Terr} * \delta^{13}{}_{Terr} + F_{Mar} * \delta^{13}{}_{Mar}$$

$$F_{Terr} + F_{Mar} = 1.$$

where $\delta^{13}C_{sample}$, $\delta^{13}{}_{Terr}$ and $\delta^{13}{}_{Mar}$ are the stable carbon isotopic compositions of the bulk sample, terrigenous end-member and marine end-member, respectively while F_{Terr} and F_{Mar} are the fractions of terrigenous and marine OC, respectively.

Radiocarbon measurements show that the bulk OC present in modern surface sediments is significantly pre-aged (a few thousand years old; Tesi et al., 2013a), including event beds collected soon after recent flood events (Tesi et al., 2011). The pre-aged origin of OC likely reflects the time spent by OC_{Terr} within watersheds prior to its release into the Adriatic Sea. Thus, the OC_{Terr} occurring in modern (<20 yr) and LIA sediment can be considered virtually the same type of material given the small age gap (i.e., a few hundred years).

Finally, we compared the model outcomes from the LIA clinothem to the contemporary Adriatic deposition (Fig. 6). Specifically, we compiled surface sediments (0–1 cm) from published studies and applied the same source-apportionment model presented above. The dataset includes surface samples collected in April 2002, October 2002, February 2003 and May 2003 in the Po prodelta ($n = 94$ samples), and in the western Adriatic clinothem ($n = 161$ samples). Samples were then clustered into three classes south of the Po prodelta for direct comparison with the LIA clinothem (Fig. 5): topset ($n = 89$ samples), foreset ($n = 51$ samples) and bottomset ($n = 21$ samples).

4. Observations and discussion

4.1. LIA elemental beds and stratal architecture

We tested the lateral continuity of the elemental beds constituting the LIA clinothem by analyzing seismic data at kilometer scale off each river discharging into the western Adriatic shelf (Figs. 1, 2 and 3). Seismic-reflection terminations suggest that the LIA clinothem comprises bedsets organized in two distinctive low-angle stratal geometries: "elongated bedsets" and "wavy bedsets" in the northern and southern sector, respectively (Figs. 2, 3 and 4).

In the northern sector, bedsets elongated parallel to the coast are highlighted at their base by planar to convex-down reflections and at their top by convex-up reflections; elongated bedsets show subparallel reflections on CHIRP profiles (Fig. 2). At the base, reflections are concordant or lap down seaward at low angle (< 1°); at the top, reflections are concordant. Thicknesses of these bedsets range from 0.4–1.5 m (0.5–2 ms; Fig. 1B). Progressively younger elongated bedsets show a shingled progradational reflection configuration (Fig. 2). Each bed has an average lateral continuity of ~15 km along and ~ 8 km across the shelf clinothem (Fig. 4). Elongated bedsets are most common in the sector north of Ancona Cape. In this sector, the foreset shows an average dip of ca. 0.2° (Fig. 2).

In the southern sector, wavy bedsets show at base and top wavy subparallel reflections that converge seaward (Fig. 3). At the base, bed reflections lap on or are concordant landward and lap down seaward; at the top, bed reflections toplap or are concordant. Compared to elongated bedsets, wavy bedsets show similar thickness but smaller lateral continuity: ~0.4–1.5 m thick (Fig. 1B), up to ~7 km along-shelf, and ~ 3 km cross-shelf (Fig. 4). A minimum lateral extent was noted on the shelf offshore of the Pescara River (average 6 km and 0.5 km, along and across shelf, respectively; Figs. 1B and 4). Wavy bedsets are most common in the offshore sector south of Ancona Cape. In this sector, the foreset has an average dip of 0.8° (Fig. 3).

In summary, we have observed two distinct domains within the Adriatic muddy clinothem deposited during the LIA: the sector north of Ancona Cape hosts elongated bedsets with maximum lateral continuity, whereas in the south wavy bedsets of limited lateral continuity occur (Figs. 1B, 4). It is important to note that the LIA clinothem reaches its maximum thickness in the southern sector where the lateral continuity of the beds is at a minimum (Fig. 4). We envision that the different lateral continuity of the elemental beds within the LIA clinothem in the north and south sectors might reflect a geographically different deposition of OC_{Terr}.

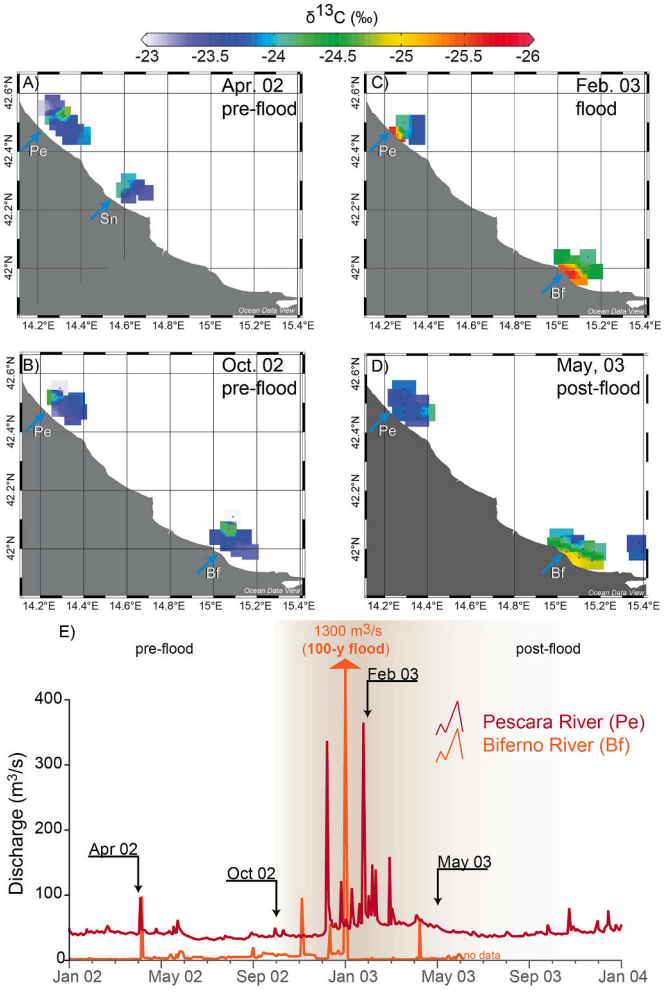

Fig. 6. $\delta^{13}C$ content in surface sediments representative of A) April 2002 pre-flood condition; B) October 2002 pre-flood condition; C) February 2003 flood event; and D) May 2003 post-flood condition. E) Hydrographs of the Pescara and Biferno rivers for 2002–2003. Arrows indicate sampling dates. Note the 100-y flood of the Biferno with 1300 m^3/s peak discharge (from Autorità di bacino del fiume Biferno, 2005, http://adbpcn.regione.molise.it/autorita/pdf/rg/biferno.pdf).

4.2. *Along-shelf OC_{Terr} redistribution vs hyperpycnal flows*

To investigate the latitudinal composition of organic material within the LIA clinothem, we selected two sediment cores representative of northern (KS02–219) and southern (KS02–357) sectors (Fig. 7) based on seismic character (Fig. 4). For these records, we quantified the relative concentration of OC_{Terr} using a source-apportionment model based on $\delta^{13}C$ (see section 3.3). Geochemical model results indicate fundamental geographical differences within LIA deposit in line with the latitudinal differences in stratal architecture and lateral continuity of beds in the LIA clinothem (Fig. 4). In particular, the average OC_{Terr} content of KS02–357 (south) is higher relative to KS02–219 (north), especially in discrete strata where OC_{Terr} can reach up to 80–90% (Fig. 7). Our terrestrial biomarker analyses confirm the $\delta^{13}C$ data indicating relatively higher OC_{Terr} concentration in the southern sector (Figs. 5 and 7). Lignin data further indicate the presence of discrete OC_{Terr}-rich strata associated with depleted $\delta^{13}C$ values (Fig. 7).

To further understand the geographical difference in the LIA clinothem and the origin of these OC_{Terr}-rich strata in the southern sector, we compared our results with the composition of modern sediments (< 20 yr) collected along the Adriatic shelf (Fig. 5). Overall, source-apportionment model outcomes show a greater fraction of OC_{Terr} accumulating in the foreset during the LIA compared to the modern sediment from the foreset (Fig. 5). This is consistent with evidence from radiocarbon-based sediment accumulation rates that suggests a much greater deposition of land-derived material during the LIA than today (Cattaneo et al., 2003).

Only flood deposits in the topset off the Biferno and Pescara river mouths exhibit a $\delta^{13}C$ signature similar to that of the OC-rich strata measured in KS02–357. These flood deposits are, however, rather ephemeral because the same topset stations, re-occupied three months after the event, did not exhibit the same depleted $\delta^{13}C$ values as those collected soon after the flood (Fig. 6). Considering the skewed nature of the Adriatic muddy clinothem, it is likely that sediments deposited in the topset are continually redistributed southward (e.g. Puig et al., 2007; Chiggiato et al., 2016) resulting in minimal long-term flood preservation. It is also likely that changes in sediment supply since the construction of dams (1948–1985; Syvitski and Kettner, 2007) have interrupted the direct supply of land-derived material to the prodelta and restricted recent flood beds geographically to the shallow topset (Fig. 6).

We infer that OC-rich strata documented in the southern LIA clinothem (KS02–357) correspond to hyperpycnal flow deposits triggered by flood events analogous to the event-driven deposition off the Biferno and Pescara river mouths despite the influence of dams (Fig. 6). Compared to these ephemeral flood deposits, however, the LIA event beds appear to be well-preserved because they reached a relatively deep region of the clinothem where post-depositional reworking is minimal (i.e., below storm wave base). Our hypothesis is strongly supported by the sedimentary analyses of the two sediment records. Specifically, in the northern sector of the LIA clinothem we observed structureless clayey sediments and/or curved laminae with possible hummocky or swaley cross-lamination (X-ray of KS02–219, Fig. 7n1-n3), typical of strata deposited under combined flows (Lazar et al., 2015). This finding is in agreement with numerical models that posited the influence of strong storm waves and faster coastal currents in the foreset of the northern sector (Harris et al., 2008). In contrast, the occurrence of preserved planar-parallel laminae to ripple cross-laminations in the southern sector (X-ray of KS02–357, Fig. 7n4-n6), coupled with a coarser sediment texture, indicates that these sediments accumulated under high-energy unidirectional flows (Schieber et al., 2007). In addition, thin-section analyses of KS02–357 show the presence of laminae successions with inverse to normal grading (Fig. 7A), typical of hyperpycnal flow deposits (Mulder et al., 2003; Zavala et al., 2011; Li et al., 2015). These laminae successions are associated with plant fragments (50 to 100 μm size) and soft and deformable intraclasts (Fig. 7B and C, respectively), and show depleted $\delta^{13}C$ values and high lignin content (Fig. 7). Alternatively, storms might have resuspended the OC_{Terr} from shallow waters but this would necessarily have remobilized a mixture of material thus diminishing the land-derived signal.

Overall, our results suggest a multifaceted scenario during the LIA wherein along-shelf sediment redistribution in the northern sector dominated over direct supply from rivers while hyperpycnal flows in the southern sector were capable of depositing event beds in the foreset (Fig. 8), which today appears to be disconnected from direct river input (Figs. 5 and 6).

4.3. *Diagnostic stratal geometries to predict the fate of OC_{Terr} and its transport time*

Our integrated analysis suggests that geometric complexity along the LIA muddy clinothem is likely a function of contrasting depositional processes which, in turn, affected the sediment redistribution and, consequently, the fate of OC_{Terr}. Structureless sediments characterized by OC enriched in $\delta^{13}C$ and low lignin contents were found in elongated bedsets (northern sector, Fig. 7) and indicate sediment redistribution along the shelf by the generally southward marine circulation (Fig. 8). During transport, reactive OC_{Terr} was likely degraded due to sustained

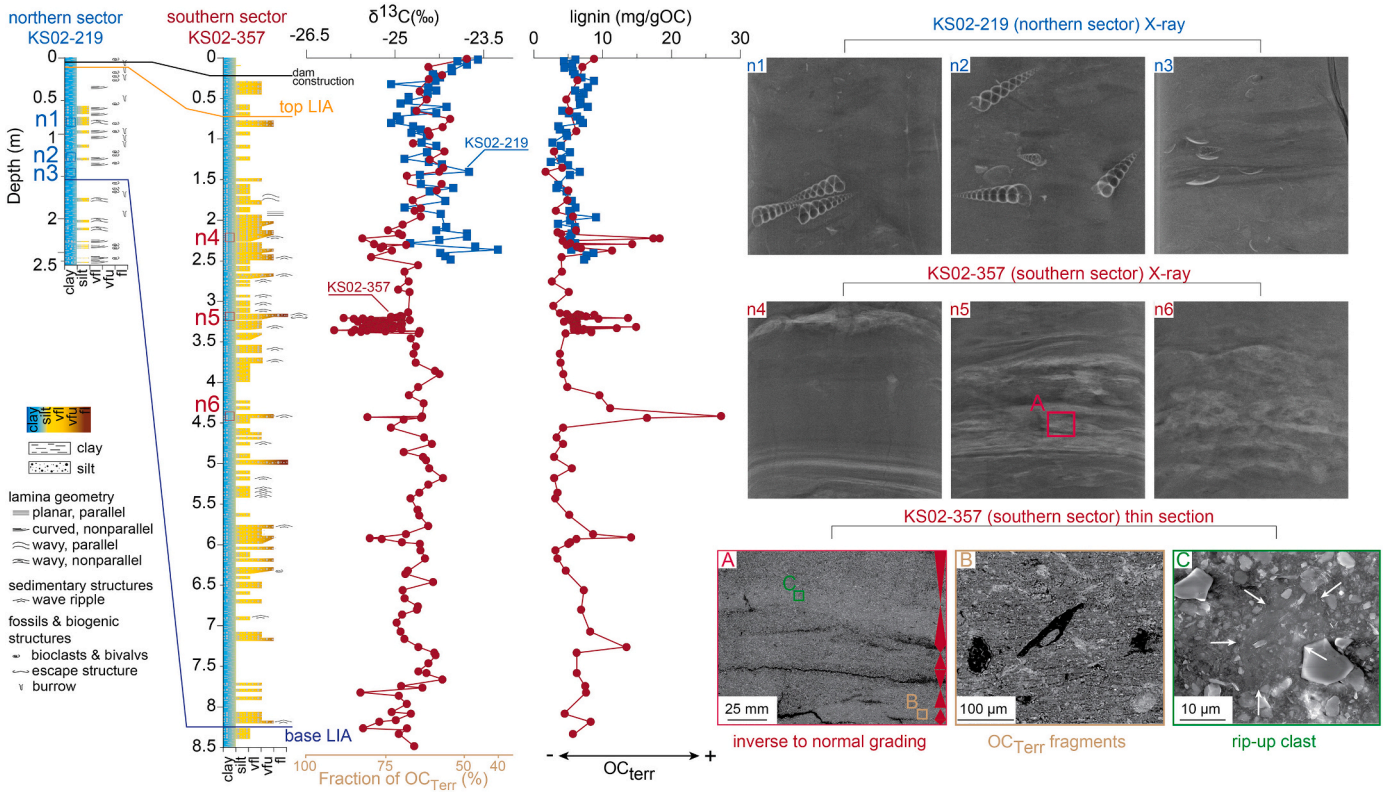

Fig. 7. From left to right: descriptive logs and grain size of cores KS02–219 and KS02–357. Orange and blue horizons represent top and base of the LIA, respectively. In the $\delta^{13}C$ and lignin content, the blue data points are from core KS02–219, and the red data points are from core KS02–357. X-ray (8 × 8 cm; upper two rows) and thin-section SEM images (bottom row) of key parts of cores KS02–219 and KS02–357 are shown in the right half of the figure. Red rectangle in X-ray image 'n5' is the area of the thin section shown in A-B-C. (A) Normal and inverse grading shown with red triangles, orange square shows location of (B), and green square shows location of (C). (B) Example of land-plant fragment (black). (C) White arrows mark fine-grained intraclasts. (For interpretation of the references to colour in this figure legend, the reader is referred to the web version of this article.)

exposure to oxic-suboxic conditions (long transport time; Fig. 8) as documented on other shelves (Keil et al., 2004; Cui et al., 2016; Bröder et al., 2018). Despite this, $\delta^{13}C$ suggests that the accumulation of OC_{Terr} in the northern sector (KS02–219) was, to some extent, more efficient during the LIA compared to the modern deposition, as expected given the different climate and level of human activity back then. Finally, it is worth mentioning that, in addition to the influence of dams previously discussed, selective degradation of marine OC during burial might partially explain the slightly more depleted $\delta^{13}C$ values in the northern LIA foreset compared to the recent accumulation.

Regarding the southern LIA clinothem, depleted $\delta^{13}C$ and high lignin content cannot simply be explained by diagenesis. The $\delta^{13}C$ and lignin anomalies, associated with laminated and coarser sediments, were found in wavy bedsets (Fig. 7), and recorded rapid burial of land-derived material as a result of river-fed hyperpycnal flows (short transport time; Fig. 8), typical of event-deposition scenarios (Wheatcroft, 2000). In these conditions, direct local supply from flood input resulted in the rapid deposition of river-borne sediments forming wavy bedsets with minimal exposure to oxygen (Fig. 8). This suggests that smaller and steeper rivers (Apennine rivers) under major flood conditions generated high-density flows that traveled quickly across the shelf to water depths that exceed wave base, implying accelerated and pulsed burial from individual catchments.

Overall, our results suggest that seismic facies analysis along an apparently uniform 600-km-long muddy clinothem can be used to predict the relative abundance, and, to some extent, infer preservation and composition of OC_{Terr} in shelfal deposits. Furthermore, elevated sediment input during the LIA (Cattaneo et al., 2003) did not necessarily translate into efficient burial of OC_{Terr} when lateral redistribution affected stratal geometries and carried sediment over long distances (northern sector; B-B′ section in Fig. 8). Our study indicates that stratal architecture and OC_{Terr} accumulation were highly coupled during the LIA (Fig. 8). This finding implies that prodeltaic undulations (sensu Urgeles et al., 2007; 2011) are indicative of rapid burial of OC_{Terr} by river-fed hyperpycnal flows on continental shelves, thus reflecting short transport time (southern sector; A-A' section in Fig. 8). Overall, this implies that OC_{Terr} deposition could be qualitatively predicted through subtle diagnostic changes in stratal geometry evidenced by high-resolution seismic stratigraphic images (Fig. 8).

4.4. The LIA deposit as analogue of ancient fine-grained systems

The relation of OM character and preservation with transport distance and duration is a key variable in reconstructing river-dominated shelf to basin systems. Mudstone-dominated strata with mixtures of terrigenous and marine organic matter of various preservation states are the dominant sedimentary rock found at the earth surface (e.g., Potter et al., 2012) and depositional variations are a key influence on the distribution of organic-matter types. Our work can provide guidance for understanding and predicting the potential of OC hot spots as well as their small-scale lateral variations in ancient shelfal mudstones. In terms of small-scale lateral variations, although the resolution of most commercially acquired multi-channel marine reflection seismic data would be insufficient to resolve the bedsets discussed in this paper, onshore 3D seismic collected over shale-gas or tight-oil fields can, in some cases, approach the required resolution (e.g., Davies et al., 2004). The observed differences in sedimentary features among muddy systems in contrasting depositional scenarios (Fig. 8) might also be useful to the improved interpretation of ancient fine-grained successions (e.g. Cretaceous Western Interior Seaway of North America, Bhattacharya

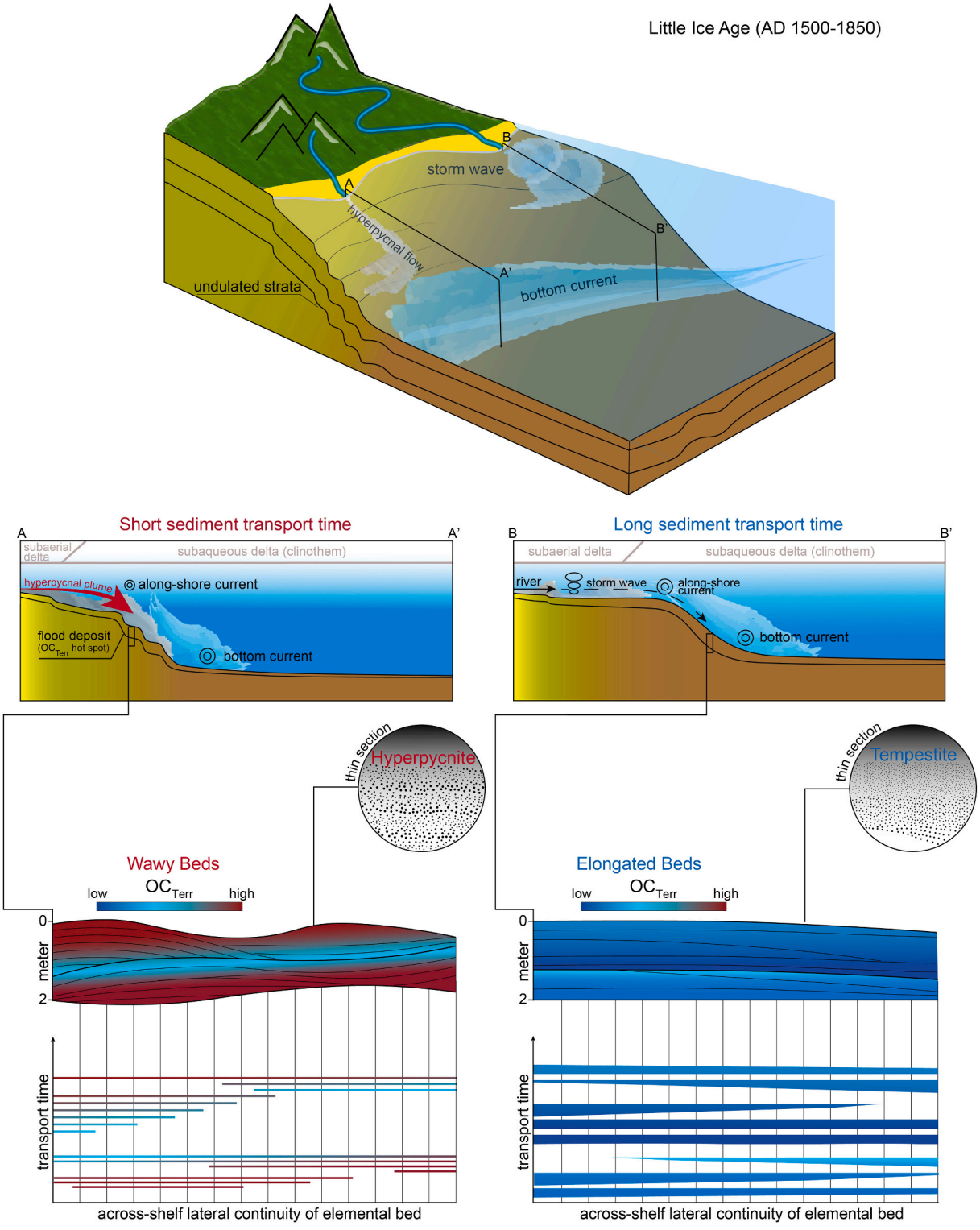

Fig. 8. Top: conceptual sketch showing the fundamental mechanisms governing the fate of land-derived material on the shelf during the Little Ice Age (LIA); note the closer proximity of mountains and coastline to a steeper prodelta in the southern sector. Bottom current flows parallel to the coastline reshaping sediment in both sectors. Central: idealized A-A' section, hyperpycnal flows from local rivers overwhelm along-shelf redistribution (despite some sediment reshaping by bottom-current) which results in preservation of OC_{Terr}, suggesting a depositional environment consistently connected to terrigenous sediment source (southern sector); idealized B-B′ section, sediment redistribution along the shelf prevails over the local river sediment input, which results in poor preservation of flood events and OC_{Terr} (northern sector). Bottom: 4-D Wheeler diagram (sensu Qayyum et al., 2015) showing stratal geometry as a diagnostic tool to predict the time spent under oxic condition and the fate of OC_{Terr}. Stratigraphic architecture (top) and chronostratigraphic charts (bottom) of the elemental bedsets constitute the LIA clinothem. Wavy elemental beds show reduced across-shelf (along-dip/basinward direction) continuity and virtually nil transport time (faster deposition = thin bars in the chronostratigraphic chart), resulting in deposits with higher OC_{Terr} preservation; elemental beds of greater lateral continuity define elongated bedsets and reflect long-distance transport resulting in deposits with lower OC_{Terr} content. Insets represent schematic illustration of sedimentary structures and grain-size variation at thin-section scale.

and MacEachern, 2009, Hampson, 2010, Li et al., 2015; Eocene Central Basin of Spitsbergen, Plink-Björklund, 2020; and Pliocene Orinoco Delta of the Trinidad Basin, Peng et al., 2018, 2020). Post-depositional compaction, however, may obscure originally visible geometries and may render hummocky or swaley lamina styles as well as wavy bedsets as apparently parallel. Nonetheless, key features of these geometries, such as lateral termination at lamina, bed, and larger scales can still be recognized in ancient deposits (e.g. Schieber et al., 2007; Yawar and Schieber, 2017), and together with "virtual decompaction" of digital images (Lobza and Schieber, 1999) allow their restoration for comparison with modern muds.

Well logs have appropriate vertical resolution (ca. 30 cm) and where well spacing is sufficiently close, such subtle small-scale stratal geometries can be recognized and mapped. For example, Fig. 9 portrays an ancient example of an analogous mudstone-dominated shelfal setting, the mid-Cretaceous Mowry and Belle Fourche shales in the Bighorn Basin, Wyoming, USA. This ancient example resembles the Adriatic margin because the strata accumulated in a closed-ended shallow seaway developed in a foreland basin (Armstrong and Oriel, 1965) on a muddy shelf that was mostly storm-wave dominated with intervals and areas of river-flood dominance (Bohacs et al., 2005, 2009a, 2009b, 2021). This interval comprises a mix of moderately to poorly preserved marine OM and a variety of terrigenous OM types (Bohacs et al., 2021). These strata accumulated in association with coeval shallow-marine siliciclastic shorelines to the west and northwest (e.g., Bohacs et al., 2021).

The cross section is oriented along the dominant sediment transport direction and is at a scale roughly equivalent to the high-resolution seismic lines through the Adriatic LIA strata. Elemental beds average slightly less than 1 m thick (range: 0.3—1.8 m); bedsets average 2.8 m thick (range: 1.5—5.0 m); lateral continuity ranges from ≤3.5 km (around well 1804) to ≥13 km. The well-log correlations portray intricate stratal geometries comparable to the LIA interval, with closely spaced small-scale truncation, onlap, and downlap of strata of equivalent scale to 'elemental beds' organized into larger-scale bedsets in aggradational and progradational stacking patterns. At the base of bedsets, beds lap on or are concordant landward and mostly lap down basinward. At top, beds are commonly truncated, with a few being concordant. The area around well 1804 (Fig. 9) demonstrates numerous stratal terminations at multiple levels and synoptic erosional relief of up to 4 m over 1 to 2 km lateral distances. We interpret this reach to represent a river-flood dominated area of an overall storm-wave-dominated shelf with local influx of terrigenous sediment and elevated OC_{Terr}, analogous to the Adriatic wavy bedsets.

For areas with coarser-resolution seismic or more widely spaced wells what can inform predictions are our insights that OC type and preservation can vary laterally over hundreds of meters to a few km (Fig. 4), and that OC_{Terr} preservation is a function of not only distance from a river mouth, sediment supply, and shelf width (e.g. Sweet and Blum, 2016; Walsh and Nittrouer, 2009; Covault and Graham, 2010), but also transport duration and depositional environment. In particular, the LIA clinothem indicates higher preservation potential in area with steeper foresets located at water depths below storm wave base, and in strongly coupled river–shelf systems (Fig. 8).

5. Conclusions

Integrated observations across a wide range of stratigraphic and sedimentological scales (from km to μm) accompanied by geochemical analyses allow prediction of the variation in lateral transport and preservation of sedimentary organic carbon along the apparently uniform 600-km-long fine-grained deposit of the west Adriatic shelf. From analyzing these LIA strata, we infer that the burial efficiency of OC_{Terr} along the shelf varies as a function of sediment transport processes which, in turn, can be inferred from stratal geometries at seismic to core and thin-section scales. Rapid emplacement in the southern sector, driven by hyperpycnal flows, generated maximum complexity of stratal geometry (wavy bedsets, multiple short-spaced stratal terminations, and limited bed continuity) and resulted in efficient sequestration of OC_{Terr}. By contrast, protracted sediment transport along the northern sector of the Adriatic shelf (long-distance transport) generated broader stratal geometries (elongated bedsets, extended stratal continuity) characterized by reduced preservation of OC_{Terr} despite the relative short distance from river mouths.

Our results indicate that subtle stratal geometries can be used as a diagnostic proxy to predict differences in accumulation of OC_{Terr} even in

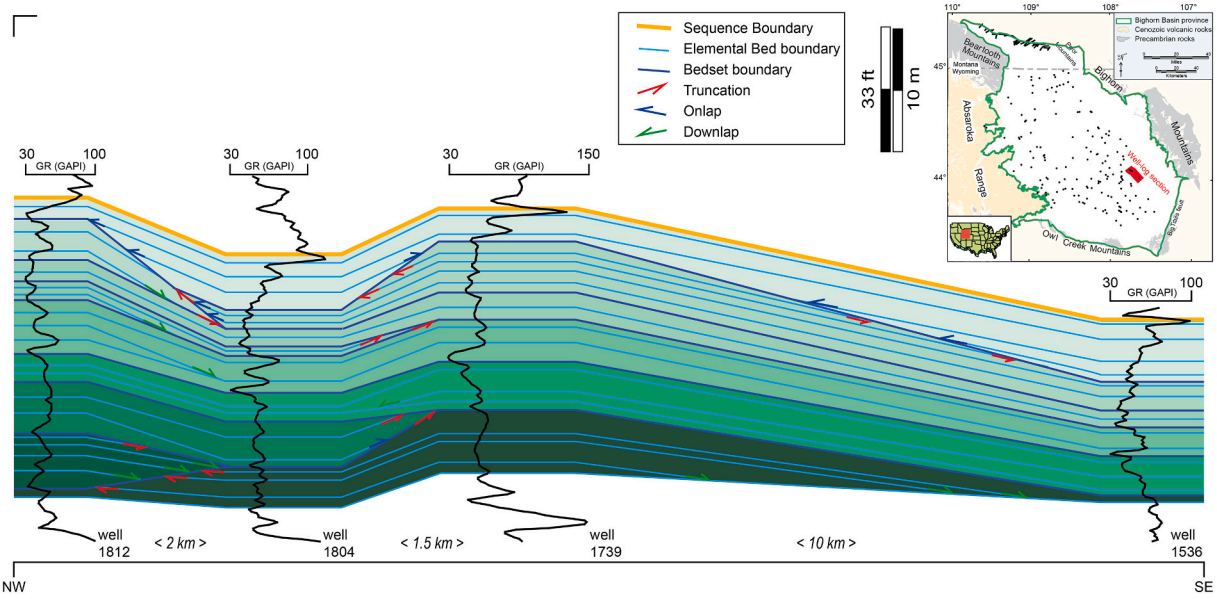

Fig. 9. Well-log cross section parallel to dominant sediment transport direction of an analogous mudstone-dominated shelfal setting, the Cretaceous (u. Albian to Cenomanian) Mowry depositional sequence that spans the upper interval of the Mowry Shale and the Belle Fourche Shale in the Bighorn Basin, Wyoming-Montana, USA. High-resolution well-log correlations portray intricate stratal geometries comparable to the Adriatic LIA interval, with closely spaced small-scale truncation, onlap, and downlap of strata of equivalent scale to 'elemental beds' organized into larger-scale bedsets in aggradational and shingled progradational stacking patterns. GR: gamma-ray log in API units. Orange line at top of cross section is a regionally extensive erosional unconformity.

a depositional system like a muddy subaqueous clinothem that, at basin scale, appears homogenous. Overall, our findings imply that muddy deposits characterized by high sedimentation rates do not necessarily lead to high OC_{Terr} burial because specific sediment transport processes exert first-order control on OC_{Terr} fate. This finding confirms the importance of understanding the details of lateral heterogeneity of sedimentary archives and strata-hosted resources. Global carbon inventories as well as paleoenvironmental reconstructions of fine-grained rock accumulations would benefit from accounting for such subtle lateral heterogeneities to explain variations in OC content at <1 km scale. Finally, paleogeographic reconstructions based on OC_{Terr} content of offshore mudstones should also take into consideration the non-conservative nature of OC_{Terr} which varies as a function of post-depositional processes as well as the lateral transport time of sediment redistribution.

Declaration of Competing Interest

The authors declare that they have no known competing financial interests or personal relationships that could have appeared to influence the work reported in this paper.

Acknowledgments

This contribution is part of a project funded by PRIN-MIUR ("The Po-Adriatic Source-to-Sink system (PASS): from modern sedimentary processes to millennial-scale stratigraphic architecture"), contract 2017ASZAKJ_001 to A. Amorosi. Editor Liviu Matenco and three anonymous Reviewers are thanked for insightful comments that improved the paper. A special thanks to Jacopo Chiggiato for useful discussion on the Adriatic oceanographic regime. We thank Andrea Gallerani for X-ray scans and Luigi Vigliotti and Sonia Albertazzi for SIRM and ^{210}Pb data, respectively. This is ISMAR-CNR contribution number 2053.

Appendix B. Supplementary data

Supplementary data to this article can be found online at https://doi.org/10.1016/j.gloplacha.2021.103539.

References

Aller, R.C., Blair, N.E., 2006. Carbon remineralization in the Amazon–Guianas tropical mobile mudbelt: a sedimentary incinerator. Cont. Shelf Res. 26 (17–18), 2241–2259.
Amorosi, A., Maselli, V., Trincardi, F., 2016. Onshore to offshore anatomy of a late quaternary source-to-sink system (Po Plain–Adriatic Sea, Italy). Earth Sci. Rev. 153, 212–237.
Anthony, E.J., Marriner, N., Morhange, C., 2014. Human influence and the changing geomorphology of mediterranean deltas and coasts over the last 6000 years: from progradation to destruction phase? Earth Sci. Rev. 139, 336–361.
Armstrong, F.C., Oriel, S.S., 1965. Tectonic development of Idaho-Wyoming thrust belt. AAPG Bull. 49 (11), 1847–1866.
Artegiani, A., Paschini, E., Russo, A., Bregant, D., Raicich, F., Pinardi, N., 1997. The Adriatic Sea general circulation. Part I: air – sea interactions and water mass structure. J. Phys. Oceanogr. 27, 1492–1514.
Bao, R., McIntyre, C., Zhao, M., Zhu, C., Kao, S.J., Eglinton, T.I., 2016. Widespread dispersal and aging of organic carbon in shallow marginal seas. Geology 44 (10), 791–794.
Bao, R., Uchida, M., Zhao, M., Haghipour, N., Montlucon, D., McNichol, A., Eglinton, T.I., 2018. Organic carbon aging during across-shelf transport. Geophys. Res. Lett. 45 (16), 8425–8434.
Bauer, J.E., Cai, W.-J., Raymond, P.A., Bianchi, T.S., Hopkinson, C.S., Regnier, P.A., 2013. The changing carbon cycle of the coastal ocean. Nature 504, 61–70.
Benetazzo, A., Bergamasco, A., Bonaldo, D., Falcieri, F.M., Sclavo, M., Langone, L., Carniel, S., 2014. Response of the Adriatic Sea to an intense cold air outbreak: dense water dynamics and wave-induced transport. Prog. Oceanogr. 128, 115–138.
Bentley, S.J., Nittrouer, C.A., 2003. Emplacement, modification, and preservation of event strata on a flood-dominated continental shelf: eel shelf, northern California. Cont. Shelf Res. 23 (16), 1465–1493.
Berner, R.A., 1982. Burial of organic carbon and pyrite sulfur in the modern ocean: its geochemical and environmental significance. Am. J. Sci. 282, 451–473.
Bhattacharya, J.P., MacEachern, J.A., 2009. Hyperpycnal rivers and prodeltaic shelves in the Cretaceous seaway of North America. J. Sediment. Res. 79 (4), 184–209.
Bianchi, T.S., Wysocki, L.A., Schreiner, K.M., Filley, T.R., Corbett, D.R., Kolker, A.S., 2011. Sources of terrestrial organic carbon in the Mississippi plume region: evidence for the importance of coastal marsh inputs. Aquat. Geochem. 17 (4), 431–456.
Bianchi, T.S., Schreiner, K.M., Smith, R.W., Burdige, D.J., Woodard, S., Conley, D.J., 2016. Redox effects on organic matter storage in coastal sediments during the Holocene: a biomarker/proxy perspective. Annu. Rev. Earth Planet. Sci. 44, 295–319.
Bianchi, T.S., Cui, X., Blair, N.E., Burdige, D.J., Eglinton, T.I., Galy, V., 2018. Centers of organic carbon burial and oxidation at the land-ocean interface. Org. Geochem. 115, 138–155.
Blair, N.E., Aller, R.C., 2012. The fate of terrestrial organic carbon in the marine environment. Annu. Rev. Mar. Sci. 4, 401–423.
Bohacs, K.M., Grabowski, G.J.J., Carroll, A.R., Mankiewicz, P.J., Miskell-Gerhardt, K.J., Schwalbach, J.R., Wegner, M.B., Andsimo, J.A., 2005. Production, destruction, and dilution: the many paths to source-rock development. In: Harris, N.B. (Ed.), The Deposition of Organic-Carbon-Rich Sediments: Models, Mechanisms, and Consequences: SEPM, Special Publication, 82, pp. 61–101.
Bohacs, K.M., Casell, E., Hemmisch, N., Jonk, R., Lazar, O.R., MacQuaker, J.H.S., 2009a. Significant variations in hydrocarbon source and mudstone-reservoir character at the parasequence scale: counter-intuitive trends, systematic relations, and economic implications: Annual Meeting Expanded Abstracts. American Association of Petroleum Geologists.
Bohacs, K.M., MacQuaker, J.H.S., Lazar, O.R., Jonk, R., Hemmesch, N., Cassel, E.J., 2009b. Detailed anatomy of parasequences in mudstone-dominated, allegedly anoxic settings; examples from the Cretaceous Mowry Shale and associated formations, Western U.S.. In: Abstracts: Annual Meeting – American Association Of Petroleum Geologists.
Bohacs, K.M., Lazar, O.R., Wilson, R.D., Macquaker, J.H.S., 2021. Mowry Shale—Belle Fourche Shale, Bighorn Basin, Wyoming, USA—Mesozoic clastic-biosiliceous shelf system, a prolific source rock with associated mudstone reservoir potential, Chapter 12. In: Bohacs, K.M., Lazar, R. (Eds.), Sequence Stratigraphy: Applications to Fine-Grained Rocks: AAPG Memoir, 126 in press.
Bornhold, B.D., Prior, D.B., 1990. Morphology and sedimentary processes on the subaqueous Noeick River delta, British Columbia, Canada. In: Spec. Publs int. Ass. Sediment., vol 10 IAS, pp. 169–181. https://doi.org/10.1002/9781444303858.ch9.
Bröder, L., Tesi, T., Andersson, A., Semiletov, I., Gustafsson, Ö., 2018. Bounding cross-shelf transport time and degradation in Siberian-Arctic land-ocean carbon transfer. Nat. Commun. 9 (1), 806.
Broecker, W.S., 2000. Was a change in thermohaline circulation responsible for the Little Ice Age? Proc. Natl. Acad. Sci. 97 (4), 1339–1342.
Cai, W.J., 2011. Estuarine and coastal ocean carbon paradox: CO2 sinks or sites of terrestrial carbon incineration? Annu. Rev. Mar. Sci. 3, 123–145.
Campbell, C.V., 1967. Lamina, laminaset, bed, and bedset. Sedimentology 8, 7–26.
Camuffo, D., Secco, C., Brimblecombe, P., Martin-Vide, J., 2000. Sea storms in the Adriatic Sea and the Western Mediterranean during the last millennium. Clim. Chang. 46 (1–2), 209–223.
Cattaneo, A., Correggiari, A., Langone, L., Trincardi, F., 2003. The late-Holocene Gargano subaqueous delta, Adriatic shelf: sediment pathways and supply fluctuations. Mar. Geol. 193, 61–91.
Cattaneo, A., Correggiari, A., Marsset, T., Thomas, Y., Marsset, B., Trincardi, F., 2004. Seafloor undulation patterns on the Adriatic shelf and comparison to deep-water sediment waves. Mar. Geol. 213, 121–148.
Cattaneo, A., Trincardi, F., Asioli, A., Correggiari, A., 2007. The western Adriatic shelf clinoform: energy-limited bottomset. Cont. Shelf Res. 27, 506–525.
Chiggiato, J., Bergamasco, A., Borghini, M., Falcieri, F.M., Falco, P., Langone, L., Miserocchi, S., Russo, A., Schroeder, K., 2016. Dense-water bottom currents in the Southern Adriatic Sea in spring 2012. Mar. Geol. 375, 134–145. https://doi.org/10.1016/j.margeo.2015.09.005.
Comiti, F., 2012. How natural are Alpine mountain rivers? Evidence from the Italian Alps. Earth Surf. Process. Landf. 37 (7), 693–707.
Correggiari, A., Trincardi, F., Langone, L., Roveri, M., 2001. Styles of failure in late holocene highstand prodelta wedges on the Adriatic shelf. J. Sediment. Res. 71 (2), 218–236. https://doi.org/10.1306/042800710218.
Covault, J.A., Graham, S.A., 2010. Submarine fans at all sea-level stands: tectono-morphologic and climatic controls on terrigenous sediment delivery to the deep sea. Geology 38 (10), 939–942.
Cui, X., Bianchi, T.S., Hutchings, J.A., Savage, C., Curtis, J.H., 2016. Partitioning of organic carbon among density fractions in surface sediments of Fiordland, New Zealand. J. Geophys. Res. Biogeosci. 121, 1016–1031.
Davies, R.J., Stewart, S.A., Cartwright, J.A., Lappin, M., Johnston, R., Fraser, S.I., Brown, A.R., 2004. 3D seismic technology: are we realising its full potential? Geol. Soc. Lond. Mem. 29 (1), 1–10.
Denommee, K.C., Bentley, S.J., Harazim, D., Macquaker, J.H., 2016. Hydrodynamic controls on muddy sedimentary-fabric development on the Southwest Louisiana subaqueous delta. Mar. Geol. 382, 162–175.
Dezileau, L., Sabatier, P., Blanchemanche, P., Joly, B., Swingedouw, D., Cassou, C., Von Grafenstein, U., 2011. Intense storm activity during the Little Ice Age on the French Mediterranean coast. Palaeogeogr. Palaeoclimatol. Palaeoecol. 299 (1–2), 289–297.
Fagan, B., 2019. The Little Ice Age: How Climate Made History 1300–1850. Hachette UK.
Fanget, A.-S., Bern, é S., Jouet, G., Bassetti, M.-A., Dennielou, B., Maillet, G.M., Tondut, M., 2014. Impact of relative sea level and rapid climate changes on the architecture and lithofacies of the Holocene Rhone subaqueous delta (Western Mediterranean Sea). Sediment. Geol. 305, 35–53. https://doi.org/10.1016/j.sedgeo.2014.02.004.

Frignani, M., Langone, L., Ravaioli, M., Sorgente, D., Alvisi, F., Albertazzi, S., 2005. Fine sediment mass balance in the western Adriatic continental shelf over a century time scale. Mar. Geol. 222–223, 113–133.
Giosan, L., Coolen, M.J., Kaplan, J.O., Constantinescu, S., Filip, F., Filipova-Marinova, M., Thom, N., 2012. Early anthropogenic transformation of the Danube-Black sea system. Sci. Rep. 2, 582.
Goñi, M.A., Monacci, N., Gisewhite, R., Crockett, J., Nittrouer, C., Ogston, A., Aalto, R., 2008. Terrigenous organic matter in sediments from the fly river delta-clinoform system (Papua New Guinea). J. Geophys. Res. Earth Surf. 113 (F1).
Gordon, E.S., Goñi, M.A., 2003. Sources and distribution of terrigenous organic matter delivered by the Atchafalaya River to sediments in the northern Gulf of Mexico. Geochim. Cosmochim. Acta 67 (13), 2359–2375.
Grove, A.T., 2001. The" Little Ice Age" and its geomorphological consequences in Mediterranean Europe. Clim. Chang. 48 (1), 121–136.
Hampson, G.J., 2010. Sediment dispersal and quantitative stratigraphic architecture across an ancient shelf. Sedimentology 57 (1), 96–141.
Harris, C.K., Sherwood, C.R., Signell, R.P., Bever, A.J., Warner, J.C., 2008. Sediment dispersal in the northwestern Adriatic Sea. J. Geophys. Res. Oceans 113 (C11).
Hedges, J.I., 1992. Global biogeochemical cycles: progress and problems. Marine chemistry 39 (1-3), 67–93.
Hedges, J.I., Keil, R.G., 1995. Sedimentary organic matter preservation: an assessment and speculative synthesis. Marine chemistry 49 (2-3), 81–115.
Hedges, J.I., Keil, R.G., Benner, R., 1997. What happens to terrestrial organic matter in the ocean? Org. Geochem. 27 (5–6), 195–212.
Keil, R.G., Dickens, A.F., Arnarson, T., Nunn, B.L., Devol, A.H., 2004. What is the oxygen exposure time of laterally transported organic matter along the Washington margin? Mar. Chem. 92 (1–4), 157–165.
Korus, J.T., Fielding, C.R., 2015. Asymmetry in Holocene river deltas: patterns, controls, and stratigraphic effects. Earth Sci. Rev. 150, 219–242.
Kulkarni, C., Peteet, D.M., Boger, R., 2018. The Little Ice Age and human-environmental interactions in the Central Balkans: insights from a new Serbian paleorecord. Quat. Int. 482, 13–26.
Lazar, O.R., Bohacs, K.M., Schieber, J., Macquaker, J.H., Demko, T.M., 2015. Mudstone Primer: Lithofacies Variations, Diagnostic Criteria, and Sedimentologic-Stratigraphic Implications at Lamina to Bedset Scales. SEPM (Society for Sedimentary Geology).
Lee, S.H., Chough, S.K., 2001. High-resolution (2–7 kHz) acoustic and geometric characters of submarine creep deposits in the South Korea Plateau, East Sea. Sedimentology 48 (3), 629–644. https://doi.org/10.1046/j.1365-3091.2001.00383.x.
Lee, H.J., Syvitski, J.P.M., Parker, G., Orange, D., Locat, J., Hutton, E.W.H., Imran, J., 2002. Distinguishing sediment waves from slope failure deposits: field examples, including the 'Humboldt slide', and modeling results. Mar. Geol. 192 (1–3), 79–104. https://doi.org/10.1016/S00253227(02)00550-9.
Li, Z., Bhattacharya, J., Schieber, J., 2015. Evaluating along-strike variation using thin-bedded facies analysis, Upper Cretaceous Ferron Notom Delta, Utah. Sedimentology 62 (7), 2060–2089.
Liu, J.P., Milliman, J.D., Gao, S., Cheng, P., 2004. Holocene development of the Yellow River's subaqueous delta, North Yellow Sea. Mar. Geol. 209 (1–4), 45–67.
Lobza, V., Schieber, J., 1999. Biogenic sedimentary structures produced by worms in soupy, soft muds; observations from the Chattanooga Shale (Upper Devonian) and experiments. J. Sediment. Res. 69 (5), 1041–1049.
Luisetti, T., Ferrini, S., Grilli, G., Jickells, T.D., Kennedy, H., Kröger, S., Tyllianakis, E., 2020. Climate action requires new accounting guidance and governance frameworks to manage carbon in shelf seas. Nat. Commun. 11 (1), 1–10.
Mariani, G.S., Compostella, C., Trombino, L., 2019. Complex climate-induced changes in soil development as markers for the Little Ice Age in the Northern Apennines (Italy). Catena 181, 104074.
Maselli, V., Trincardi, F., 2013. Man made deltas. Sci. Rep. 3, 1926.
McClain, M.E., Boyer, E.W., Dent, C.L., Gergel, S.E., Grimm, N.B., Groffman, P.M., Hart, S.C., Harvey, J.W., Johnston, C.A., Mayorga, E., 2003. Biogeochemical hot spots and hot moments at the interface of terrestrial and aquatic ecosystems. Ecosystems 6, 301–312.
Michels, K.H., Kudrass, H.R., Hu, C., 1998. The submarine delta of the Ganges–Brahmaputra: cyclone-dominated sedimentation patterns. Mar. Geol. 149, 133–154.
Mulder, T., Syvitski, J.P., Migeon, S., Faugeres, J.C., Savoye, B., 2003. Marine hyperpycnal flows: initiation, behavior and related deposits, A review. Mar. Pet. Geol. 20 (6–8), 861–882.
Nittrouer, C.A., Kuehl, S.A., Figueiredo, G., Allison, M.A., Sommerfield, C.K., Rine, J.M., Faria, T.L.E.C., Silveira, O.M., 1996. The geological record preserved by Amazon shelf sedimentation. Cont. Shelf Res. 16, 817–841.
Oldfield, F., Asioli, A., Accorsi, C.A., Mercuri, A.M., Juggins, S., Langone, L., Rolph, T., Trincardi, F., Wolff, G., Gibbs, Z., Vigliotti, L., Frignani, M., Van der post, K., Branch, N., 2003. A high resolution late Holocene palaeo environmental record from the central Adriatic Sea. Quat. Sci. Rev. 22, 319–342.
Palinkas, C.M., Nittrouer, C.A., 2006. Clinoform sedimentation along the Apennine shelf, Adriatic Sea. Mar. Geol. 234 (1–4), 245–260.
Patruno, S., Helland-Hansen, W., 2018. Clinoforms and clinoform systems: review and dynamic classification scheme for shorelines, subaqueous deltas, shelf edges and continental margins. Earth Sci. Rev. 185, 202–233.
Patruno, S., Hampson, G.J., Jackson, C.A., 2015. Quantitative characterization of deltaic and subaqueous clinoforms. Earth Sci. Rev. 142, 79–119.
Pellegrini, C., Maselli, V., Cattaneo, A., Piva, A., Ceregato, A., Trincardi, F., 2015. Anatomy of a compound delta from the post-glacial transgressive record in the Adriatic Sea. Mar. Geol. 362, 43–59.
Pellegrini, C., Patruno, S., Helland-Hansen, W., Steel, R., Trincardi, F., 2020. Clinoforms and clinothems: fundamental elements of basin infill. Basin Res. https://doi.org/10.1111/bre.12446.
Peng, Y., Steel, R.J., Olariu, C., 2018. Amazon fluid mud impact on tide-and wave-dominated Pliocene lobes of the Orinoco Delta. Mar. Geol. 406, 57–71.
Peng, Y., Steel, R.J., Olariu, C., Li, S., 2020. Rapid subsidence and preservation of fluvial signals in an otherwise wave-reworked delta front succession: early-mid Pliocene Orinoco continental-margin growth, SE Trinidad. Sediment. Geol. 395, 105,555.
Pirmez, C., Pratson, L.F., Steckler, M.S., 1998. Clinoform development by advection-diffusion of suspended sediment: modeling and comparison to natural systems. J. Geophys. Res. Solid Earth (1978–2012) 103 (B10), 24,141–24,157.
Piva, A., Asioli, A., Trincardi, F., Schneider, R.R., Vigliotti, L., 2008. Late-Holocene climate variability in the Adriatic Sea (Central Mediterranean). The Holocene 18 (1), 153–167.
Plink-Björklund, P., 2020. Shallow-water deltaic clinoforms and process regime. Basin Res. 32, 251–262 (Clinoforms and Clinothems: Fundamental Elements of Basin Infill).
Potter, P.E., Maynard, J.B., Pryor, W.A., 2012. Sedimentology of Shale: Study Guide and Reference Source. Springer-Verlag, New York, p. 303, 1980.
Poulain, P.M., 2001. Adriatic sea surface circulation as derived from drifter data between 1990 and 1999. J. Mar. Syst. 29 (1–4), 3–32.
Puig, P., Ogston, A.S., Guillén, J., Fain, A.M.V., Palanques, A., 2007. Sediment transport processes from the topset to the foreset of a crenulated clinoform (Adriatic Sea). Cont. Shelf Res. 27 (3–4), 452–474.
Qayyum, F., De Groot, P., Hemstra, N., Catuneanu, O., 2015. 4D Wheeler diagrams: concept and applications. Geol. Soc. Lond., Spec. Publ. 404 (1), 223–232.
Renaud, F.G., Syvitski, J.P., Sebesvari, Z., Werners, S.E., Kremer, H., Kuenzer, C., Friedrich, J., 2013. Tipping from the Holocene to the Anthropocene: how threatened are major world deltas? Curr. Opin. Environ. Sustain. 5 (6), 644–654.
Schieber, J., 2013. SEM observations on ion-milled samples of devonian black shales from Indiana and New York: the petrographic context of multiple pore types. AAPG Mem. 102, 153–172.
Schieber, J., Southard, J.B., Thaisen, K.G., December 14, 2007. Accretion of mudstone beds from migrating floccule ripples. Science 318, 1760–1763, 37(6), 483–486.
Schimmelmann, A., Riese, David J., Schieber, Juergen, 2015. Fast and economical sampling and resin-embedding technique for small cores of unconsolidated, fine-grained sediment. In: 2015 Pacific Climate (PACLIM) Workshop, 8–11 March, Asilomar Conference Grounds, Pacific Grove, California, pp. 50–51 (abstracts).
Slootman, A., Cartigny, M.J., 2020. Cyclic steps: review and aggradation-based classification. Earth Sci. Rev. 201, 102,949.
Smith, R.W., Bianchi, T.S., Allison, M., Savage, C., Galy, V., 2015. High rates of organic carbon burial in fjord sediments globally. Nat. Geosci. 450–453.
Sweet, M.L., Blum, M.D., 2016. Connections between fluvial to shallow marine environments and submarine canyons: implications for sediment transfer to deep water. J. Sediment. Res. 86 (10), 1147–1162.
Syvitski, J.P., Kettner, A.J., 2007. On the flux of water and sediment into the Northern Adriatic Sea. Cont. Shelf Res. 27 (3–4), 296–308.
Syvitski, J.P., Kettner, A., 1938. 2011, Sediment flux and the Anthropocene. Philosophical Transactions of the Royal Society A: Mathematical, Physical and Engineering Sciences 369, 957–975.
Syvitski, J.P., Vörösmarty, C.J., Kettner, A.J., Green, P., 2005. Impact of humans on the flux of terrestrial sediment to the global coastal ocean. Science 308 (5720), 376–380.
Tesi, T., Miserocchi, S., Langone, L., Boni, L., Guerrini, F., 2006. Sources, fate and distribution of organic matter on the western Adriatic Continental shelf, Italy. Water, Air, Soil Pollut. Focus 6, 593–603.
Tesi, T., Miserocchi, S., Goñi, M.A., Turchetto, M., Langone, L., De Lazzari, A., Albertazzi, S., Correggiari, A., 2011. Influence of distributary channels on sediment and organic matter supply in event-dominated coastal margins: the Po prodelta as a study case. Biogeosciences 8, 365–385.
Tesi, T., Langone, L., Goñi, M.A., Wheatcroft, R.A., Miserocchi, S., Bertotti, L., 2012. Early diagenesis of recently deposited organic matter: a 9-yr time-series study of a flood deposit. Geochim. Cosmochim. Acta 83, 19–36.
Tesi, T., Langone, L., Giani, M., Ravaioli, M., Miserocchi, S., 2013a. Source, diagenesis, and fluxes of particulate organic carbon along the western Adriatic Sea (Sea). Mar. Geol. 337, 156–170.
Tesi, T., Miserocchi, S., Acri, F., Langone, L., Boldrin, A., Hatten, J.A., Albertazzi, S., 2013b. Flood-driven transport of sediment, particulate organic matter, and nutrients from the Po River watershed to the Mediterranean Sea. J. Hydrol. 498, 144–152.
Traykovski, P., Wiberg, P.L., Geyer, W.R., 2007. Observations and modeling of wave-supported sediment gravity flows on the Po prodelta and comparison to prior observations from the Eel shelf. Cont. Shelf Res. 27 (3–4), 375–399.
Trincardi, Fabio, Amorosi, Alessandro, Bosman, Alessandro, Correggiari, Anna, Madricardo, Fantina, Pellegrini, Claudio, 2020. Ephemeral rollover points and clinothem evolution in the modern Po Delta based on repeated bathymetric surveys. Basin Research 402–418. https://doi.org/10.1111/bre.12426.
Trincardi, F., Normark, W., 1988. Sediment waves on the Tiber prodelta slope: interaction of deltaic sedimentation and currents along the shelf. Geo-Mar. Lett. 8 (3), 149–157. https://doi.org/10.1007/bf02326091.
Urgeles, R., De Mol, B., Liquete, C., Canals, M., De Batist, M., Hughes-Clarke, J.E., Amblás, D., Arnau, P.A., Calafat, A.M., Casamor, J.L., Centella, V., De Rycker, K., Fabrés, J., Frigola, J., Lafuerza, S., Lastras, G., Sánchez, A., Zuñiga, D., Versteeg, W., Willmott, V., 2007. Sediment undulations on the Llobregat prodelta: signs of early slope instability or sedimentary bedforms? J. Geophys. Res. 112.
Urgeles, R., Cattaneo, A., Puig, P., Liquete, C., DE Mol, B., Ambl, à s D., Sultan, N., Trincardi, F., 2011. A review of undulated sediment features on Mediterranean

prodeltas: distinguishing sediment transport structures from sediment deformation. Mar. Geophys. Res. 32 (1), 49–69. https://doi.org/10.1007/s11001-011-9125-1.
Van Wagoner, J.C., Mitchum, R.M., Campion, K.M., Rahmanian, V.D., 1990. Siliciclastic sequence stratigraphy in well logs, cores, and outcrops: concepts for high-resolution correlation of time and facies.
Vigliotti, L., Verosub, K., Cattaneo, A., Trincardi, F., Asioli, A., Piva, A., 2008. Palaeomagnetic and rock magnetic analysis of Holocene deposits from the Adriatic Sea: detecting and dating short-term fluctuations in sediment supply. The Holocene 18, 141–152.
Walsh, J.P., Nittrouer, C.A., Palinkas, C.M., Ogston, A.S., Sternberg, R.W., Brunskill, G.J., 2004. Clinoform mechanics in the Gulf of Papua, New Guinea. Continental Shelf Research 24 (19), 2487–2510.
Walsh, J.P., Nittrouer, C.A., 2009. Understanding fine-grained river-sediment dispersal on continental margins. Mar. Geol. 263 (1–4), 34–45.
Wheatcroft, R.A., 2000. Oceanic flood sedimentation: a new perspective. Cont. Shelf Res. 20 (16), 2059–2066.
Xue, Z., Liu, J.P., DeMaster, D., Van Nguyen, L., Ta, T.K.O., 2010. Late Holocene evolution of the Mekong subaqueous delta, southern Vietnam. Mar. Geol. 269 (1–2), 46–60.
Yawar, Z., Schieber, J., 2017. On the origin of silt laminae in laminated shales. Sediment. Geol. 360, 22–34.
Zavala, C., Arcuri, M., Di Meglio, M., Gamero Diaz, H., Contreras, C., 2011. A genetic facies tract for the analysis of sustained hyperpycnal flow deposits. In: Slatt, R.M., Zavala, C. (Eds.), Sediment Transfer from Shelf to Deep Water—Revisiting the Delivery System: AAPG Studies in Geology, 61, pp. 31–51.
Zonneveld, K.A.F., Versteegh, G.J.M., Kasten, S., Eglinton, T.I., Emeis, K.C., Huguet, C., Koch, B.P., de Lange, G.L., de Leeuw, J.W., Middelburg, J.J., Mollenhauer, G., Prahl, G.H., Rethemeyer, J., Wakeham, S.G., 2010. Selective preservation of organic matter in marine environments; processes and impact on the sedimentary record. Biogeosciences 7 (2), 483–511.